Exp Fluids (2015) 56:169
DOI 10.1007/s00348-015-2038-z

RESEARCH ARTICLE

Comparison between velocity- and vorticity-based POD methods in a turbulent wake

S. L. Tang[1,2] · L. Djenidi[2] · R. A. Antonia[2] · Y. Zhou[1]

Received: 22 January 2015 / Revised: 29 July 2015 / Accepted: 2 August 2015 / Published online: 11 August 2015

Abstract In this paper, the velocity-based POD and the vorticity-based POD have been systematically compared in three characteristic regions of the flow downstream of a two-dimensional circular cylinder, namely the near, intermediate and far wakes. The two-point space correlation function is used to determine which of the two methods is better suited for extracting the large-scale flow structures based on the repartition of energy among the different POD modes. It is found that the POD, based on the lateral velocity fluctuation v, leads to the most optimum extraction in all three flow regions, while the vorticity-based POD is only effective in the near and intermediate wakes. Based on two-point space correlation functions, a scenario is proposed for the application of POD to the present two-dimensional wake.

1 Introduction

Coherent structures (CS), which are commonly regarded as vortices, turn out to be of paramount importance not only for understanding turbulence phenomena such as mixing and entrainment, mass and heat transfer, drag, lift and aerodynamic noise generation, but also for the viable modeling of turbulence. Therefore, the identification and extraction of CS in turbulent flows is a necessary first step, which in turn necessitates an objective and unbiased method of extraction of the CS in the turbulent flow fields. The proper orthogonal decomposition (POD) method has become a well-established tool used for identifying these structures since it was first introduced by Lumley (1967).

The characteristic feature of the conventional POD is that it can capture the contribution of the most energetic structures to the turbulent kinetic energy in the first few modes. Therefore, if the dynamics of the flow is dominated by a few large flow structures containing most of the energy, it can often be represented satisfactorily by using only a few of the first modes of the POD. These modes will then reflect the energetic structures. This velocity-based POD has been applied in many turbulent flows, such as flow around a vibrating cantilever (Kim et al. 2011), a cavity flow (Murray et al. 2009), the axisymmetric wake behind a disk (Johansson et al. 2002), the flow past a backward-facing step (Kostas et al. 2002), the turbulent jet in crossflow (Meyer et al. 2007), an internal combustion engine flow (Fogleman et al. 2004), a turbulent planar jet (Gordeyev and Thomas 2000) and a channel flow (Duggleby et al. 2007). They all indicated that the velocity-based POD helps in extracting useful information associate with CS from the complex flow fields.

In the last decade, there has been increasing interest in applying vorticity-based POD, based on enstrophy considerations, in various turbulent flows. For example, Liberzon et al. (2005) applied the POD method to the three-dimensional vorticity field of a turbulent channel flow, obtained from direct numerical simulation (DNS) data. Extraction of the essential features of the coherent structures is achieved through a linear combination of the first vorticity-based

✉ S. L. Tang
shunlin.tang88@gmail.com

L. Djenidi
lyazid.djenidi@newcastle.edu.au

1 Institute for Turbulence-Noise-Vibration Interaction and Control, Shenzhen Graduate School, Harbin Institute of Technology, Shenzhen 518055, People's Republic of China

2 Discipline of Mechanical Engineering, School of Engineering, The University of Newcastle, Callaghan, NSW 2308, Australia

POD modes. Gurka et al. (2006) presented a direct comparison of the vorticity-based POD with the velocity-based POD modes using particle image velocimetry (PIV) in the streamwise wall-normal plane of a fully developed turbulent boundary layer in a flume. The results showed that an unambiguous CS emerges only by utilizing the vorticity-based POD. They inferred that it is due to the fact that vorticity is Galilean invariant and is linked directly to the coherent structures. Kostas et al. (2005) performed POD on both the fluctuating velocity and vorticity fields of a backward-facing step flow at Reynolds numbers of 580 and 4660, based on step height and freestream velocities. The data were obtained from PIV measurements. They observed that the vorticity-based POD captured the fluctuation enstrophy, which is the square of vorticity [see Eq. (1)], more efficiently than the velocity-based POD. Hence, they suggested that POD modes obtained from the vorticity-based decomposition will be more effective in the study of flow structures. Joshi et al. (2009) and Tabib and Joshi (2008) further inferred that this is due to the fact that a higher value of enstrophy indicates the presence of organized structures, but the same may not be guaranteed from larger values of the kinetic energy [square of velocity, see Eq. (2)].

$$\zeta = \omega_i \cdot \omega_i = \sum \omega_i^2 \tag{1}$$

$$k = u_i \cdot u_i = \sum u_i^2, \tag{2}$$

where ω_i and u_i are the fluctuating components of vorticity and velocity, respectively. Although the vorticity-based POD has been found to be more efficient for extracting energetically dominant modes than the velocity-based POD in several flows, the vorticity-based POD performed in the flow fields inside a street canyon (Kellnerova et al. 2012) showed that every mode contributes just a little to the total enstrophy, i.e., no dominant mode emerged. On the contrary, the velocity-based POD performed in the same flow fields exhibited such a high relative contribution in the most dominant mode (e.g., 30–40 %), showing that the flow is highly organized. In addition, Feng et al. (2011) applied both the vorticity-based POD and the velocity-based POD to the wake of a circular cylinder with synthetic jet control and showed that the POD results based on streamwise and vertical velocities are similar to those from the vorticity-based POD for different vortex shedding regimes. It thus seems that the type of POD that is better suited for extracting the dominant structures may depend on the particular flow. One question naturally arises. Is there a criterion we can use for determining which POD is better suited to a certain flow field? The present work aims at a full comparison between velocity-based POD and vorticity-based POD in different regions of a turbulent wake, namely the near wake dominated by the von Kármán vortex street, the intermediate wake characterized by the gradual disappearance of the von Kármán vortices and the far wake which is approximately self-preserving, e.g., Townsend (1956). The results are analyzed with the aim to propose a criterion which can determine which POD is better for extracting information about the most dominant flow structures in these different regions. The focus is not on the dynamical significance of the large-scale flow structures (or CS), but only on their extraction.

In the next section, we introduce the experimental and numerical details. A short introduction to POD is given in Sect. 3. The velocity-based POD is compared with the vorticity-based POD in Sect. 4. Conclusions are in Sect. 5.

2 Experimental details

Experiments were conducted in a closed circuit wind tunnel with a 5.0-m-long working section (0.8 m × 1.0 m). A circular cylinder of $d = 10$ mm in diameter was mounted horizontally across the working section, resulting in an aspect ratio of 80. Figure 1 shows schematic arrangement and coordinate axis. The origin of the coordinate system is defined at the mid span of the cylinder axis, with x and y along the streamwise and transverse directions, respectively. Experiments were carried out at a freestream velocity $U_\infty = 8.7$ m/s, corresponding to a Reynolds number $Re = U_\infty d/\nu = 5800$, where ν is the kinematic viscosity of fluid. A DANTEC standard PIV system was used to measure the instantaneous flow field, which was seeded by smoke, generated from paraffin oil, the averaged particle size being around 1 μm in diameter. Flow illumination was

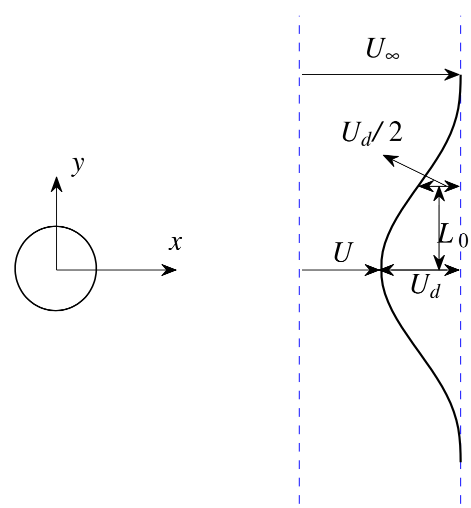

Fig. 1 Schematic arrangement and coordinate axis

provided by a double-pulse laser source with a wavelength of 532 nm. Particle images were taken using one CCD camera (double frames, 2560 × 1280 pixels) with a recording frequency of 727 Hz. The view window of the camera covers the area of $x/d = 4$–15 and $y/d = -3$ to 3, which represents the typical near wake of a cylinder; $x/d = 36$–47 and $y/d = -4$ to 4, which represents the typical intermediate wake and the area of $x/d = 400$–411 and $y/d =$ 6 to 6, which represents the typical far wake. A total of 2000 PIV image pairs were obtained for each measurement plane. The time between images of an image pair was set to be much smaller than 1/727 Hz. We checked the convergence of the mean streamwise velocity U and u' at $x/d = 7$ and $y/d = 0.9$ and found that the statistics of U and u' are converging with 600 images (not shown). Thus, 2000 image pairs are deemed to be sufficient for the present POD analysis.

3 POD

In this section, the POD is presented briefly. The basic idea of POD, when it is applied to a nonhomogeneous fluctuation field $f(x)$, is to find the linear sum of empirical functions $\Phi(x)$ which are orthogonal, i.e.,

$$f(x,t) = \sum_k a_k(t)\Phi_k(x), \tag{3}$$

$f(x)$ can be either the fluctuating velocity field or the fluctuating vorticity field. When the fluctuating velocity distributions are used as input (velocity-based POD), the resulting POD modes $\Phi_k(x)$ are an optimal decomposition in terms of TKE. If the fluctuating vorticity is used as input (vorticity-based POD), the resulting modes are optimal in terms of enstrophy. By correctly ordering the input quantities, which are the velocity (u and v) or vorticity (ω_z) in two-dimensional flow fields, into a matrix A following the snapshot method proposed by Sirovich (1987), the problem simplifies to finding

$$A^{\mathrm{T}}Av = \lambda v, \tag{4}$$

where λ are the eigenvalues and v the eigenvectors of $A^{\mathrm{T}}Av$; $A^{\mathrm{T}}Av$ is the two-point space correlation tensor in matrix form given by the products of the fluctuation part of the vorticities or velocities at different spatial locations. Ordering the solutions of Eq. (4) according to the size of the eigenvalues λ^k, the POD modes can be calculated using

$$\Phi_k(x) = \frac{1}{\sqrt{\lambda_k}}Av_k \tag{5}$$

where the first few modes are the most energetic modes. Projecting $f(x)$ onto the POD modes, we can obtain the POD coefficients that express the importance of the different modes

$$a_k(t) = \Phi_k^{\mathrm{T}}(x)f(x,t). \tag{6}$$

4 Comparison between velocity- and vorticity-based PODs

4.1 Near wake

Figure 2 shows the distribution of energy among the POD modes in the region $x/d = 4$–15 and $y/d = -3$ to 3. Hereafter, the velocity-based POD means that both u and v are used as input [see Eq. (3)] to do the POD analysis, whereas the u- or v-based POD means that either u or v is used as input. For both PODs, the first two modes contain about 70 % of the energy, while the remaining energy is shared mostly between the third and tenth modes; the contribution of modes beyond the tenth is practically negligible. Thus, the first two modes, which are associated with large-scale coherent structures as illustrated in Fig. 3, dominate the flow field.

It can be seen in Fig. 3 that the first mode of the vorticity-based POD exhibits similar spatial features than those of the second mode. This is in good agreement with the results of Ma et al. (2000), Dipankar et al. (2007) and Konstantinidis et al. (2007). Similar observations can be made for velocity-based POD. The average vortex wavelength $\lambda_c = U_c f_s$ (U_c is the convection velocity defined as $0.86U_\infty$ and f_s is the vortex shedding frequency at $x/d = 10$ (Zhou et al. 2002; Zhou and Antonia 1992) for both PODs is equal to $4.2d$.

Konstantinidis et al. (2007) showed that a symmetric distribution of the POD modes with respect to the centerline reflects the antisymmetric characteristic of the flow field (with respect to the flow centerline). Consequently, the first two modes of both PODs, illustrated in Fig. 3, are

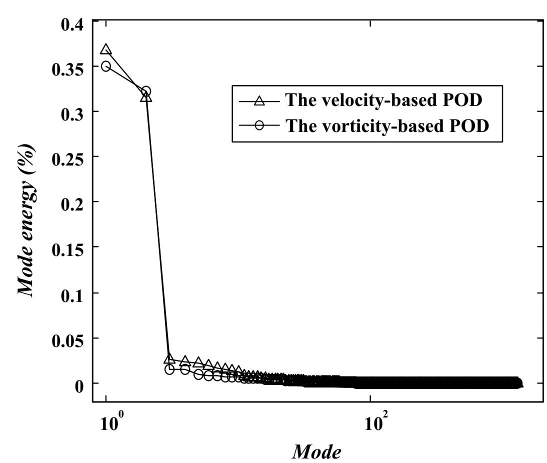

Fig. 2 Relative contribution of the individual POD modes the near wake

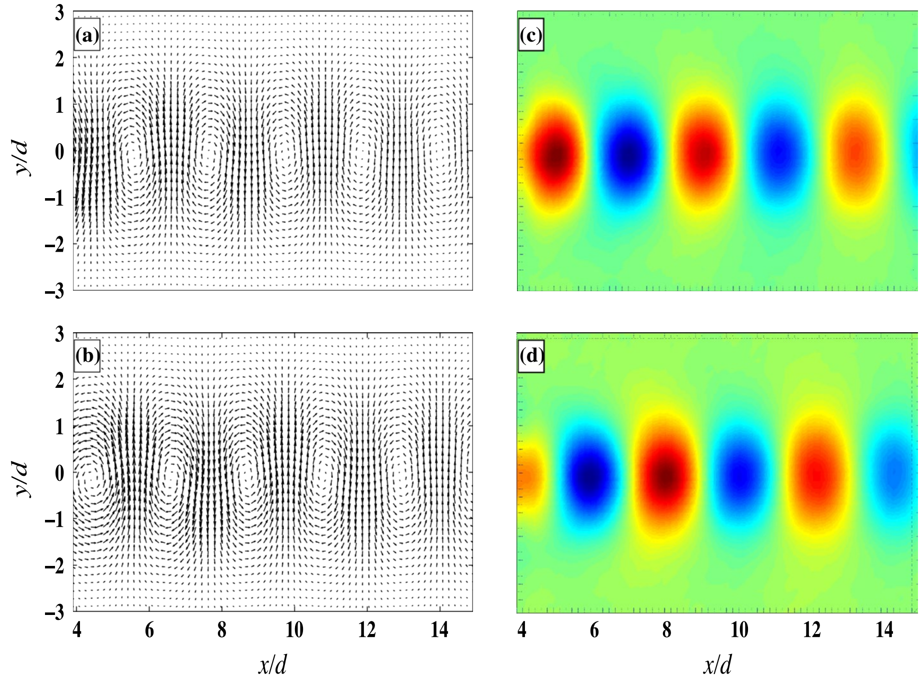

Fig. 3 First two POD modes in the near wake. **a**, **b** Velocity-based POD; **c**, **d** vorticity-based POD. **a** and **c** correspond to the first mode; **b** and **d** correspond to the second mode

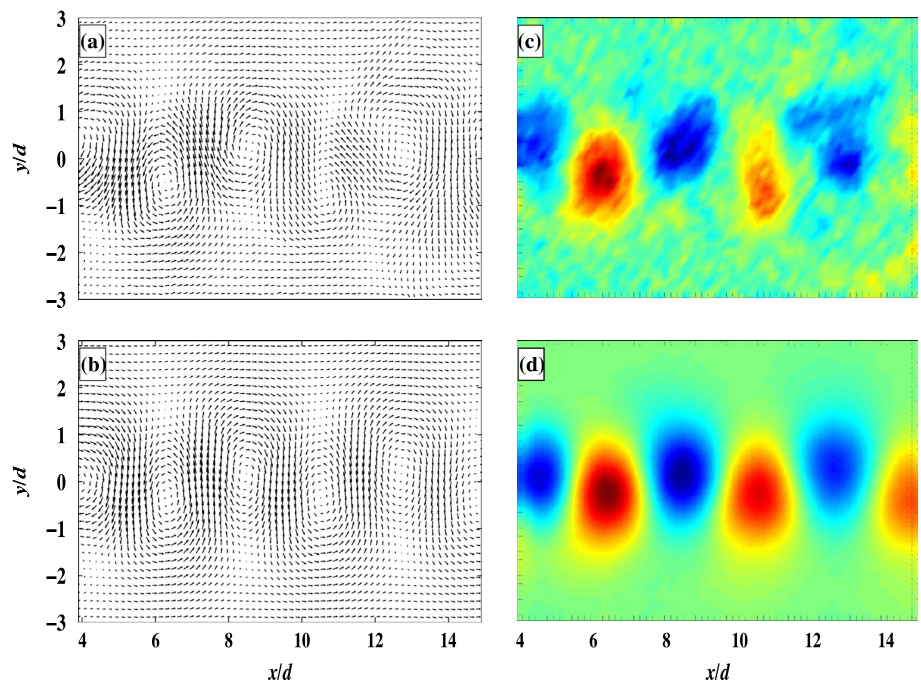

Fig. 4 **a** Typical instantaneous near wake velocity field; **b** reconstructed velocity field with the first two modes; **c** typical instantaneous vorticity field; **d** reconstructed vorticity field with the first two modes. Note that for **a**–**d**, mean values of the velocity and vorticity are added, and for **a** and **b**, $U_c = 0.86U_\infty$ at $x/d = 10$ is removed

associated with the von Kármán vortex street. This can be further validated by reconstructing the velocity and vorticity fields based on the first two modes only (see Fig. 4). These fields show practically the same spatial organization of the von Kármán vortex street. This confirms that the vorticity-based POD is as effective as the velocity-based POD for extracting and analyzing the large-scale motion in the near wake field.

Since the present PODs are based on the two-point space correlation tensor, we can use the two-point space correlation functions to explain why both PODs can reliably extract the von Kármán vortex street. The two-point correlation functions are defined as (no summation on repeated indices)

$$R_{\alpha\alpha}(x, r) = \frac{\langle \alpha(x, t)\alpha(x + r, t)\rangle}{(\sigma(x, t))^2} \quad (7)$$

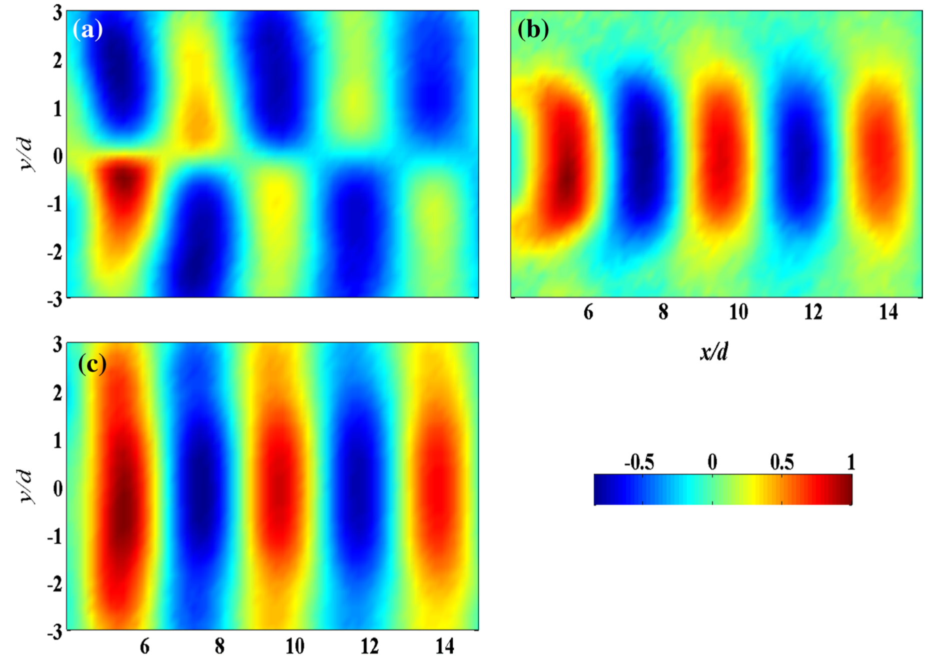

Fig. 5 Two-point correlations in near wake field. **a**R_{uu}. **b** $R_{\omega\omega}$. **c** R_{vv}

where $\alpha = u, v$ or ω_z; σ denotes the root-mean-square value of α and r is a displacement vector with its origin at x. Contours of the correlation coefficients R_{uu}, R_{vv} and $R_{\omega\omega}$ are shown in Fig. 5. All the coefficient contours present a pattern of alternate regions of positive and negative values, reflecting the strong organization of von Kármán vortex street. This may explain why the first two modes of both PODs can reflect well the large-scale von Kármán vortices.

The above analysis clearly shows that both velocity- and vorticity-based PODs can identify the large-scale motion, such as the von Kármán vortex street, in the near wake. In particular, only the first two modes of both PODs are required to achieve such a task. This is possible because the correlation coefficients R_{uu}, R_{vv} and $R_{\omega\omega}$ capture well the alternating structures of von Kármán vortex street.

Although not done here, one can perform a velocity-based POD analysis the streamwise velocity u and lateral velocity v, separately. It can be shown that combining the u- and v-based POD results leads to the same results as obtained with the velocity-based POD carried out above. This is consistent with Feng et al. (2011) who showed that the POD analysis-based one-velocity component only is appropriate for investigating the near wake.

4.2 Intermediate wake

In this section, we carry out POD analyses in the intermediate wake where the coherence of the large-scale structures is weaker than in the near wake. Accordingly, one can expect that the energy in this region is spread over a larger number of modes than in the near wake. This is indeed shown in Fig. 6.

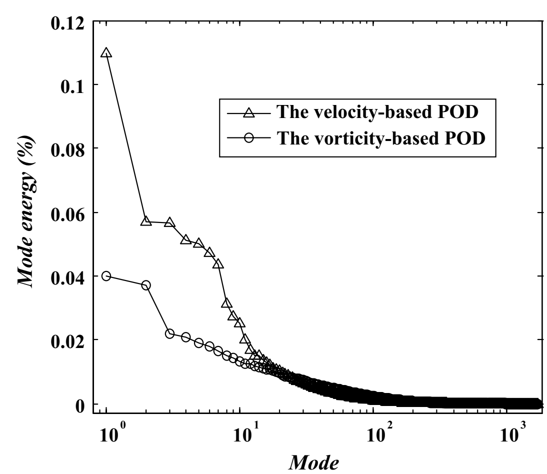

Fig. 6 Relative contribution of the individual POD modes in the intermediate wake

The energy distribution among the modes for the velocity-based POD differs significantly from that observed in the near wake. The same is seen for the enstrophy distribution. Also of interest is that while in the near wake both PODs present similar distributions, there is a marked difference in the intermediate wake. For example, the first velocity mode contains about twice the energy of the second mode, while the first and second vorticity modes have about the same enstrophy, which is about twice that of the third mode. This difference is also shown in Fig. 7, which shows the first three modes of both PODs. Notice the striking difference between the first and second velocity modes, which reflects the difference in their

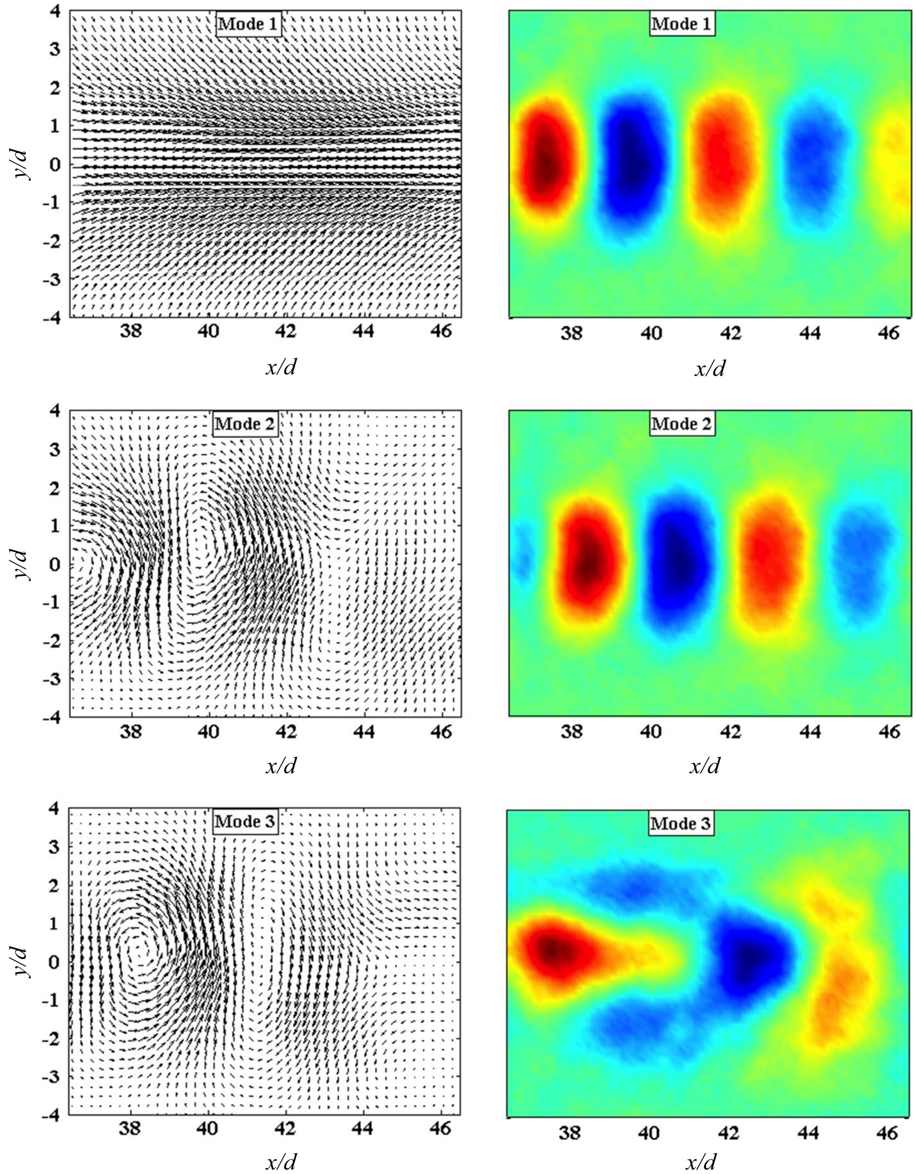

Fig. 7 First three POD modes in the intermediate wake. *Left* velocity-based POD; *right* vorticity-based POD

energy contribution. On the other hand, the second and third velocity modes are quite similar, as one may expect since they have similar energy contribution. For the vorticity-based POD, the first and second modes are similar, again reflecting similar contributions to the enstrophy. However, they differ markedly from the third mode which has a smaller enstrophy contribution. Figure 7 suggests that the von Kármán vortex street can be adequately captured by the first and second vorticity modes and to some extend the third mode. These observations are confirmed by the corresponding power spectra of the POD coefficients shown in Fig. 8. The first and second vorticity mode spectra show a clear peak at the Strouhal number $St = 0.21$ ($St = fd/U_\infty$, where f is the frequency), which corresponds to the von Kármán vortex shedding frequency at a Reynolds number of 5800 for a circular cylinder. The averaged vortex wavelength $\lambda_c = U_c f_s$, where U_c is $0.92U_\infty$ (Zhou et al. 2002), is equal to 4.38d, which is in good agreement with the value of 4.42d shown in the first two modes of the vorticity-based POD in Fig. 7. The third mode spectrum shows a clear peak at $St = 0.12$. This peak is associated with a secondary vortex street (Browne et al. 1989). The small hump for $0.2 < St < 0.3$ may be associated with vortex merging.

As hinted by Fig. 6, the velocity-based POD shows some differences with the vorticity-based POD. For example, the von Kármán vortex street is missed by the first mode but appears to be captured by the second and third modes. Also, the secondary vortex street is clearly identified in the spectra of the second and third velocity modes. Note that also the peak at $St \sim 0.2$ which is associated with the von Kármán vortex street is captured by the second and third modes. The wavelengths of modes 2 and 3 are about 6.6d

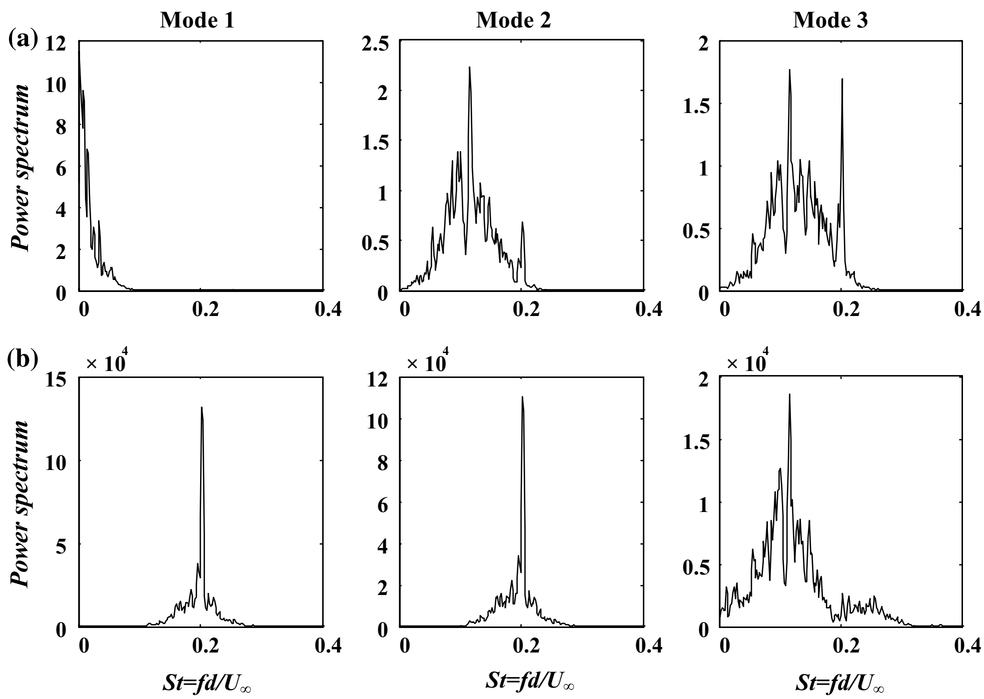

Fig. 8 Power spectra of the first three POD coefficients in the intermediate wake. **a** velocity-based POD; **b** vorticity-based POD

(see Fig. 7, right column). This is 49 % larger than the von Kármán vortex wavelength (i.e., 4.42*d*).

The reconstructed velocity and vorticity fields are shown in Fig. 9; the measured velocity field is also shown. Consistent with the above analysis, the velocity field reconstructed with the first the three modes of the velocity-based POD fails to reproduce adequately the large-scale von Kármán vortices. However, the instantaneous velocity field is sufficiently well reproduced when modes 2–10 are used. The ability of the vorticity-based POD to capture the vortical nature of the field is well demonstrated by Fig. 9d, which shows the reconstructed vorticity field using only the first two modes.

Similarly to the near wake, the two-point space correlation functions may be used to explain why the vorticity-based POD is more effective than the velocity-based POD for reflecting the existence of the coherent structures in the intermediate wake. Contours of the correlation coefficients R_{uu}, R_{vv} and $R_{\omega\omega}$ are shown in Fig. 10. The ω-correlation contours show alternating regions of positive and negative coefficients across the flow field. While the v-correlation contours exhibit a similar pattern, the u-correlation contours do not have similar alternating pattern. The lack of alternating regions of positive and negative values of R_{uu} is consistent with the failure of the velocity-based POD to represent adequately the large-scale von Kármán vortices.

Summarizing the results in the intermediate wake, one can state that the vorticity-based POD is capable of detecting the von Kármán vortex street adequately with the first two modes. On the other hand, the velocity-based POD is not as effective as the vorticity-based POD for detecting the von Kármán vortex street mainly because the u-correlation functions fail to identify the organized motions in the streamwise direction. It is worth mentioning that the v-component correlation functions can identify the organized motion, which suggests that a POD based on the velocity component v may be used to detecting the coherent motion in the intermediate wake.

4.3 Far wake

In order to further test the relative abilities of velocity- and vorticity-based PODs for extracting information on the organized motion when this latter is weak or "hidden" by the turbulence background, we carry out POD analyses in the far wake. In this region, the von Kármán vortex street has practically disappeared while quasi-organized large structures (or a secondary vortex street) prevail but are much weaker than in the near and intermediate wakes. As an example, a typical instantaneous velocity field is shown in Fig. 11. We have seen in Sects. 4.1 and 4.2 that the two-point space correlation functions could be used as a criterion for determining which of the velocity- and vorticity-based PODs is most appropriate for detecting the large-scale coherent structures. It is reasonable to assume that this can be also the case in the far wake. Accordingly, we start by

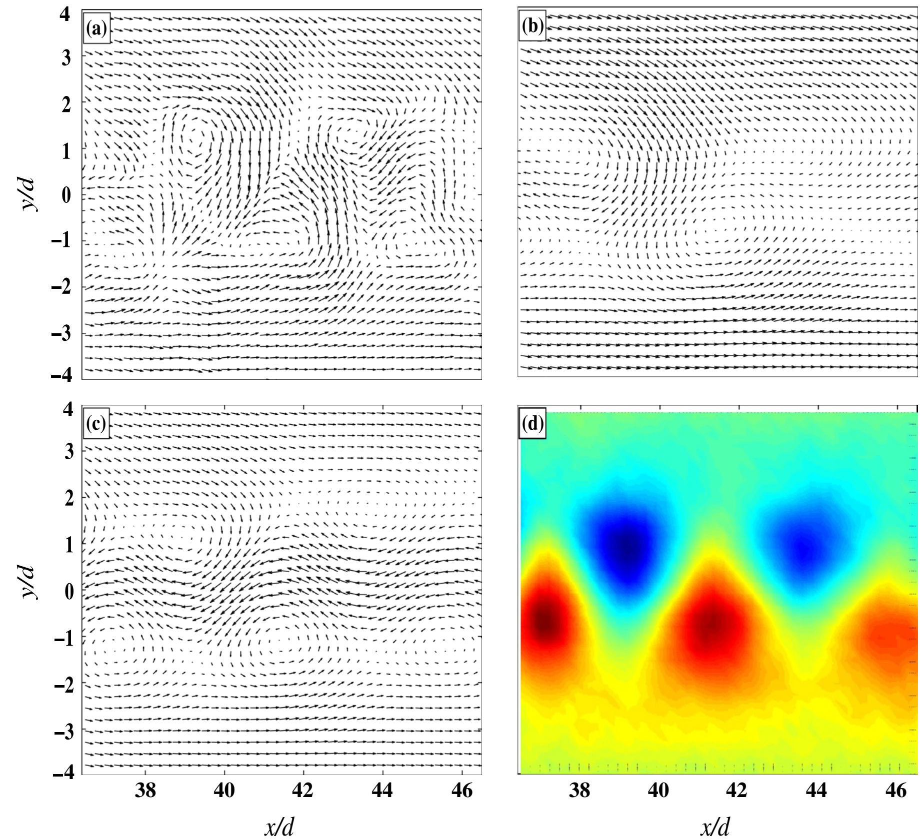

Fig. 9 **a** Typical instantaneous intermediate wake velocity field; **b** reconstructed velocity field with 1–3 modes; **b** reconstructed velocity field with 2–10 modes; **d** reconstructed vorticity field with the first two modes. Note that for **a**–**d**, mean values of the velocity and vorticity are added, and for **a**–**c**, $U_c = 92U_\infty$ at $x/d = 40$ is removed

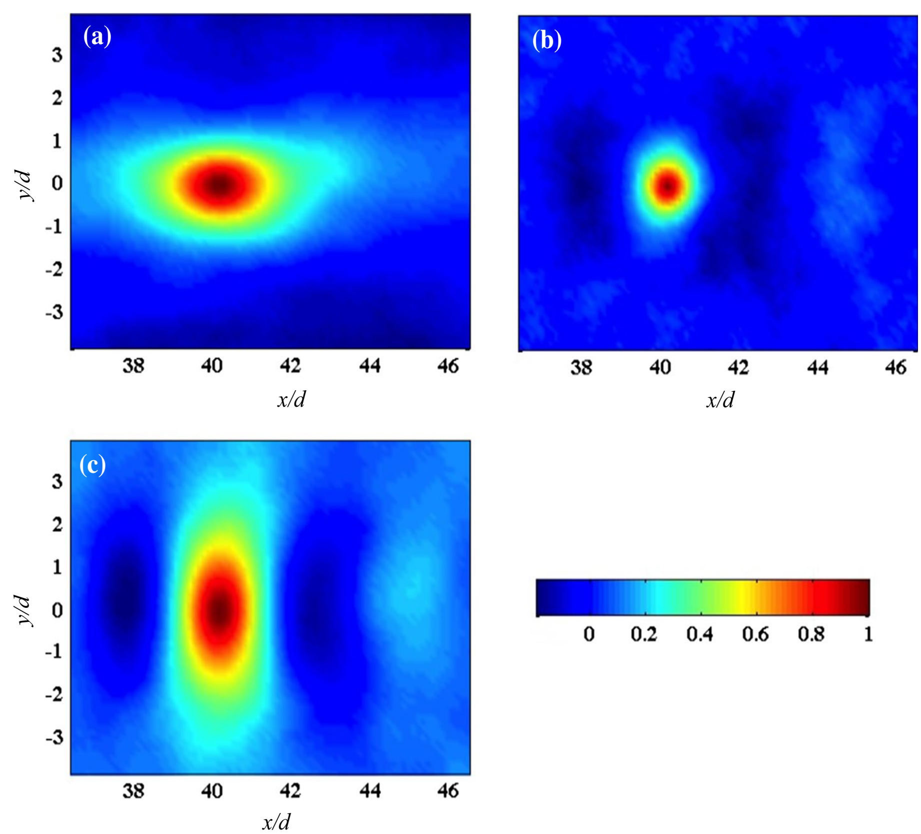

Fig. 10 Two-point correlation contours in the intermediate wake. **a** R_{uu}. **b** $R_{\omega\omega}$. **c**R_{vv}

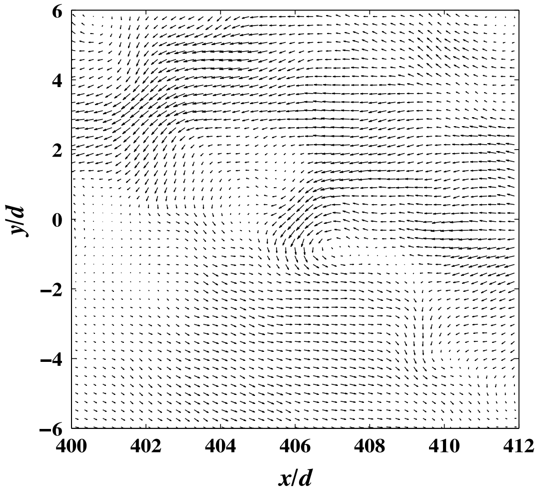

Fig. 11 Typical instantaneous far wake velocity field. $U_c = 97U_\infty$ at $x/d = 400$ is removed

calculating the correlation coefficients of R_{uu}, R_{vv} and $R_{\omega\omega}$ in the far wake before performing any POD analysis. These coefficients are shown in Fig. 12. The correlation coefficient R_{vv} presents altering elliptical shape contours similar to those observed in the intermediate wake reflecting the organization of the secondary vortex street. In contrast to R_{vv}, both R_{uu} and $R_{\omega\omega}$ have no identifiable pattern, indicating that the PODs based on the u and ω cannot detect the secondary vortex street. This is confirmed in the power spectra of the coefficients of the first and second modes shown in Fig. 13. According to Antonia and Browne (1987), the ratio of the velocity wake half-width L and λ_c is equal to about 0.23 in the far wake. None of the spectra of the first modes of the velocity- (Fig. 13a) and vorticity-based PODs (Fig. 13b) shows a clear peak around that value. Only the spectra of the coefficients for the first two modes of the v-based POD exhibit such peaks at $fL/U_c = 0.24$.

Fig. 12 Two-point correlation contours in the far wake. **a** R_{vv}. **b** R_{uu}. **c** $R_{\omega\omega}$

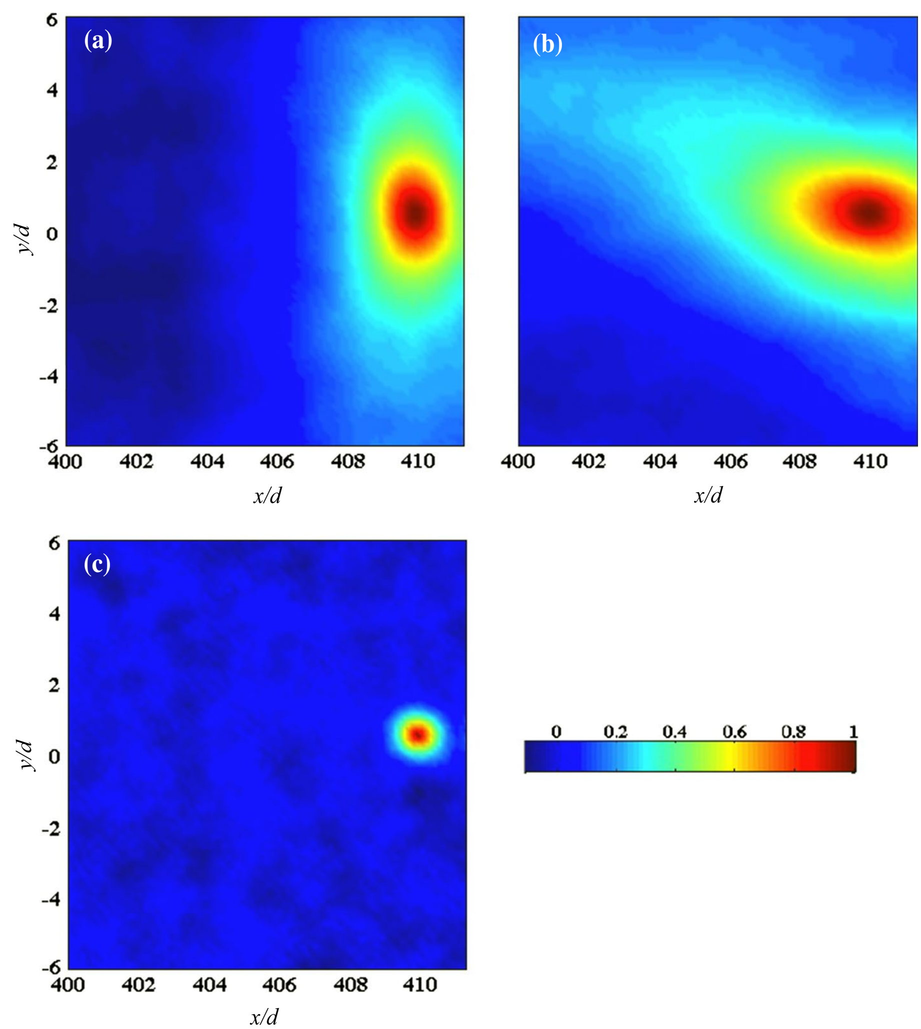

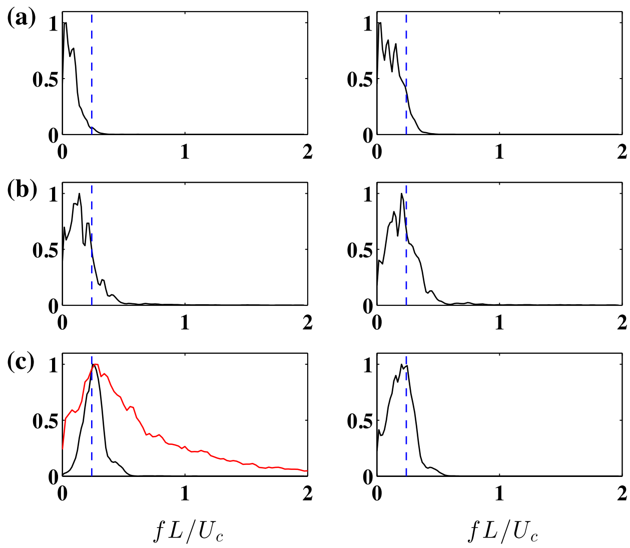

Fig. 13 Power spectra of the first two POD coefficients. **a** Velocity-based POD; **b** vorticity-based POD; **c** v-based POD. *Black curve* present data; *red curve* hot-wire on the flow centerline at $x/d = 240$ ($R_d = 1400$, Lefeuvre et al. 2014); the *vertical line* corresponds to 0.24, which is close to 0.23 (the ratio of the velocity wake half-width L and λ_c) reported by Antonia and Browne (1987). Each spectrum has been divided by its maximum value

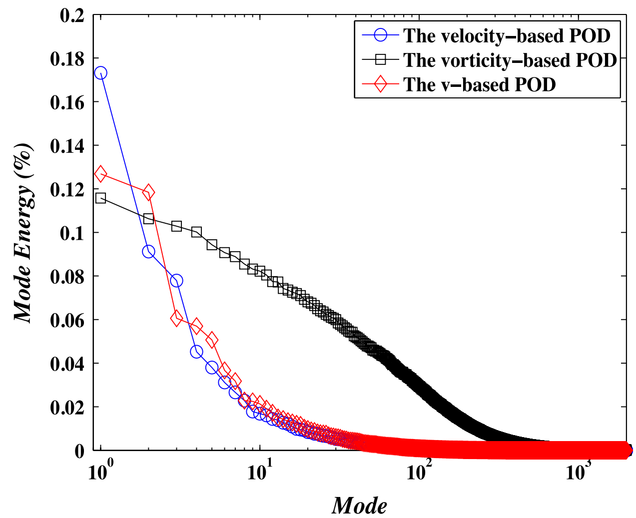

Fig. 14 Relative contribution of the individual POD modes, as a percentage of the total energy in the far wake. Note that the values for the vorticity-based POD has been multiplied by 10

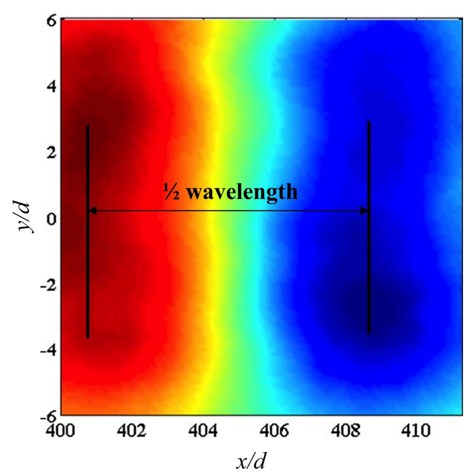

Fig. 15 First mode of the v-based POD in the far wake

Also shown in Fig. 13c is the spectrum of v, measured by hot-wire on the flow centerline at $x/d = 240$ ($R_d = 1400$). This velocity spectrum presents a peak at the frequency, $fL/U_c = 0.24$. Clearly, one may argue that the first two modes of the v-based POD can detect the organized motions well; at least it is more effective than the u- and ω-based PODs. The relative contribution of the individual POD modes are shown in Fig. 14 (the magnitude of the contribution for vorticity-based POD has been multiplied by 10). The contribution of the first u-based POD contains about 18 % of the energy. The contributions of the other modes decreases rapidly. The first and second v-based POD modes contain about 12.5 and 12 % of the energy. The contributions of the other modes is smaller and decrease rapidly too. There appears to be no dominant mode in the ω-based POD and the contribution of the individual modes decreases less rapidly than in the other two POD types.

The average wavelength of the secondary vortex street is given by

$$\lambda_c = \frac{U_c}{f_c} = \frac{0.97 U_\infty}{f_c} = 16.7d \tag{8}$$

which is in good agreement with the value of about $17d$ observed in the first mode of the v-based POD shown in Fig. 15. Antonia and Browne (1987) also measured the wavelength λ_c to be $20d$ at $x/d \approx 420$ (see also Bisset et al. 1990) which is comparable to the present value of $17d$ at $x/d \approx 405$. These comparisons further confirm that the v-based POD can capture the organization of the flow successfully in the far wake.

Hayakawa and Hussain (1989) showed that the organized structure in the nominally two-dimensional wake exhibits significant three dimensionality even in the near wake. It is reasonable to assume that this three dimensionality becomes more pronounced as x/d increases from the near wake to far wake. However, as pointed by Antonia et al. (1987), there is a reasonable similarity between the two-dimensional vector plots and flow visualization, which showed the three-dimensional nature of the flow in the far wake.

5 Conclusions

The fluctuating velocity- and fluctuating vorticity-based PODs are systematically compared in the near, intermediate and far wakes of a circular cylinder, respectively. The results show that the two-point space correlation functions could be used as a criterion for determining which POD (either velocity- or vorticity-based) is better suited for extracting the organized motion in a flow field effectively. It is found that the POD based on the lateral velocity fluctuation v leads to the most optimum extraction in all three flow regions, while the vorticity-based POD is only effective in the near and intermediate wakes.

Based on two-point space correlation functions, a scenario is also proposed for the application of POD to the present two-dimensional wake:

(a) If all the correlation coefficients R_{uu}, R_{vv} and $R_{\omega\omega}$ can identify the coherent motions, both velocity- and vorticity-based PODs can be used to detect the coherent structures.
(b) If one of the correlation coefficients fails to identify the coherent motions, say, for example, R_{uu}, but R_{vv} and $R_{\omega\omega}$ can identify the coherent motions, it is preferable to use the vorticity-based POD in order to detect the coherent structures. Note, however, that here the v-based POD can still extract the coherent motions in one direction.
(c) If both R_{uu} and $R_{\omega\omega}$ fail to identify any coherent pattern, but only R_{vv} can identify do so, we can then still extract the coherent structures using the v-based POD in one direction. These results should be of interest when the detection of weak coherent structures in the presence a background noise is to be carried out using a POD method. In such a case, our results suggest that it is best to base the POD on the v-component of the velocity.

Acknowledgments The Australian Research Council (ARC) is gratefully acknowledged for its financial support.

References

Antonia RA, Browne LWB (1987) Average wavelength of organized structures in the turbulent far wake of a cylinder. Exp Fluids 5:298–304

Antonia RA, Browne LWB, Bisset DK, Fulachier L (1987) A description of the organized motion in the turbulent far wake of a cylinder at low Reynolds number. J Fluid Mech 184:423–444

Bisset DK, Antonia RA, Browne LWB (1990) Spatial organization of large structures in the turbulent far wake of a cylinder. J Fluid Mech 218:439–461

Browne L, Antonia R, Shah D (1989) On the origin of the organised motion in the turbulent far-wake of a cylinder. Exp Fluids 7:475–480

Dipankar A, Sengupta TK, Talla SB (2007) Suppression of vortex shedding behind a circular cylinder by another control cylinder at low Reynolds numbers. J Fluid Mech 573:171–190

Duggleby A, Ball KS, Paul MR, Fischer PF (2007) Dynamical eigenfunction decomposition of turbulent pipe flow. J Turbul 8:1–24

Feng L, Wang J, Pan C (2011) Proper orthogonal decomposition analysis of vortex dynamics of a circular cylinder under synthetic jet control. Phys Fluids 23:014106

Fogleman M, Lumley J, Rempfer D, Haworth D (2004) Application of the proper orthogonal decomposition to datasets of internal combustion engine flows. J Turbul 5:N23

Gordeyev S, Thomas F (2000) Coherent structure in the turbulent planar jet. Part 1: extraction of proper orthogonal decomposition eigenmodes and their self-similarity. J Fluid Mech 414:145–194

Gurka R, Liberzon A, Hetsroni G (2006) POD of vorticity fields: a method for spatial characterization of coherent structures. Int J Heat Fluid Flow 27:416–423

Hayakawa M, Hussain F (1989) Three-dimensionality of organized structures in a plane turbulent wake. J Fluid Mech 206:375–404

Johansson PBV, George WK, Woodward SH (2002) Proper orthogonal decomposition of an axisymmetric turbulent wake behind a disk. Phys Fluids 14:2508–2514

Joshi J, Tabib M, Deshpande S, Mathpati C (2009) Dynamics of flow structures and transport phenomena, 1. Experimental and numerical techniques for identification and energy content of flow structures. Ind Eng Chem Res 48:8244–8284

Kellnerova R, Kukacka L, Jurcakova K, Uruba V, Janour Z (2012) PIV measurement of turbulent flow within a street canyon: detection of coherent motion. J Wind Eng Ind Aerodyn 63:302–313

Kim YH, Cierpka C, Werely S (2011) Flow field around a vibrating cantilerver: coherent structure eduction by continuous wavelet transform and proper orthogonal decomposition. J Fluid Mech 669:584–606

Konstantinidis E, Balabani S, Yianneskis M (2007) Bimodal vortex shedding in a perturbed cylinder wake. Phys Fluids 19(011):701

Kostas J, Soria J, Chong M (2002) Particle image velocimetry measurements of a backward-facing step flow. Exp Fluids 33:838–853

Kostas J, Soria J, Chong MS (2005) A comparison between snapshot POD analysis of PIV velocity and vorticity data. Exp Fluids 38:146–160

Lefeuvre N, Djenid L, Antonia RA, Zhou T (2014) Turbulent kinetic energy and temperature variance budgets in the far-wake generated by a circular cylinder. In: 19th Australasian fluid mechanics conference

Liberzon A, Gurka R, Tiselj I, Hetsroni G (2005) Spatial characterization of the numerically simulated vorticity fields of a flow in a flume. Theor Comput Fluid Dyn 19:115–125

Lumley JL (1967) The structure of inhomogeneous turbulent flows. In: Yaglam AM, Tatarsky VI (eds) Proceedings of the international colloquium on the fine scale structure of the atmosphere and its influence on radio wave propagation. Nauka, Moscow, pp 166–178

Ma X, Karamanos GS, Karniadakis GE (2000) Dynamics and low dimensionality of a turbulent near wake. J Fluid Mech 410:29–65

Meyer KE, Pedersen JM, Ozcan O (2007) A turbulent jet in crossflow analysed with proper orthogonal decomposition. J Fluid Mech 583:199–227

Murray N, Sallstrom E, Ukeiley L (2009) Properties of subsonic open cavity flow fields. Phys Fluids 21(095103)

Sirovich L (1987) Turbulence and the dynamics of coherent structures. Part I: coherent structures. Q Appl Math 45:561–571

Tabib MV, Joshi JB (2008) Analysis of dominant flow structures and their flow dynamics in chemical process equipment using snapshot proper orthogonal decomposition technique, chemical engineering science. Chem Eng Sci 63:3695–3715
Townsend AA (1956) The structure of turbulent shear flow, 1st edn. Cambridge University Press, Cambridge
Zhou Y, Antonia RA (1992) Convection velocity measurements in a cylinder wake. Exp Fluids 13:63–70
Zhou Y, Zhang HJ, Yiu MW (2002) The turbulent wake of two side-by-side circular cylinders. J Fluid Mech 458:303–332